Automotive Science and Engineering, Vol. 13, No. 4, (2023), 4256-4267

Iran University of Science and Technology

Automotive Science and Engineering

Journal Homepage: ase.iust.ac.ir

ISSN: 2008-9899

Development Of V-shaped plates based on the Ceramic composite for military vehicle protection

Mostafa mirtabaee[1], Mohammad abasi[2*]

[1]Shahrood University of Technology, Mechanical Engineering College

[2]Iran University of Science and Technology, School of Automotive Engineering

ARTICLE INFO

Article history:

Received : 15 Sep 2023

Accepted: 5 Dec 2023

Published: 30 Dec 2023

Keywords:

Ceramic composite

Armor vehicle

Mine explosion

Johnson-cook material model

A B S T R A C T

Protection of Armor Vehicles and military truck Occupants Against Explosion Mine and IED is the most important Parameter for comprehensive performance evaluation of armored vehicle. Armored Vehicle components Specifically Hull Floor Must be Able to Disperse Blast Shock Waves and Resist Against the structural Fracture. Analysis of the War Documents proves that flat hulls with thin-walled steel cannot resist against Anti-Tank Mines. In Recent years, development of V-shape Hull configurations Consider as an efficient Approach to improve Safety of armored vehicles. In the new generation of Armor Vehicle, Monocoque chassis combined with V-shape hull, But Replacement of All of the Old Armor Vehicle in the Defense Industry is not cost effective. So, there is an urgent need to develop the efficient strategy for enhancing the protection level of old armor vehicle. Since most of the armored vehicles used in the armies of different countries were designed and built in the past years, it is very likely that the safety standards have not been fully observed in them. Therefore, it is of great importance to provide a simple and low-cost plan for the reliable upgrade of such armored and logistics vehicles. In this article, by investigating the effect of placing V-shaped composite panels in three case studies, we were able to reduce the acceleration of the center of mass of the passenger compartment by approximately 7 times, in addition to reducing displacement by 50% on average. In addition, the explosion products were not able to penetrate into the cabin.

1. Introduction

Landmines, Improvised Explosive Devices (IEDs) and artillery shell have consistently posed a threat to armored vehicles and their occupants. It is estimated that more than half of injuries and deaths in conflict zones are caused by the detonation of landmines, particularly anti-tank (AT) mines or improvised explosive devices (IEDs). Instantaneously following the detonation, stress waves caused by the explosion propagated through the body structure, resulting in a significant deformation. Consequently, total vehicle components may be affected and accelerated upwards, posing lethal dangers to occupants [1, 2]. Consequently, armour protection is regarded as a fundamental requirement for the design of new generations of armoured vehicles USA launched Resistant Ambush Protected Programmer at the beginning of 2007 The protection level of armoured vehicle

*Corresponding Author
Email Address: mo.abasi117@gmail.com
http://doi.org/10.22068/ase.2023.655

"*Automotive Science and Engineering*" is licensed under a Creative Commons Attribution-Noncommercial 4.0 International License.

[Downloaded from i4c2023.iust.ac.ir on 2026-11-21]

[DOI: 10.22068/ase.2023.655]

occupants is also specified in the STANAG 4569 statement by the NATO Standardization Agency. STANAG 4569 identified four distinct protection levels. There are two primary methods for increasing the protection level of combat vehicles: increasing the energy absorption capability and the ability to deflect blast waves [3]. The requirements for the first level of protection can be met by a planar hull. However, it is necessary to create a more complex structure in order to achieve higher levels of security. This can be attributed to the higher explosive energy that caused shock wave permeation and intense heat, which will likely lead to the fragmentation of a single-plate structure, the transfer of energy to the occupant, and their death [4]. In order to modify the explosion response of the armored vehicles, different hall floor configurations were created. Numerous studies concentrate on the development of blast-resistant structures with enhanced explosive energy absorption capacity, such as stiffed panel, curved panel, metallic construction core, and V-shaped hull. V-shaped vessel has attracted a great deal of interest due to its exceptional characteristics, which include the ability to deflect blast waves, the reduction of vertical impulse transmission, and the prevention of blast wave interaction with the occupant zone [5]. The overall performance of an armored vehicle is typically determined by two contradictory factors: mobility and protection. Design and construction of lightweight armored vehicles are crucial to the production of armored vehicles with high mobility [6-8]. Traditional metallic alloys, such as various types of aluminum alloys and steel, require a substantial thickness for explosive protection; therefore, they cannot meet the demand for lightweight design[8]. For instance, the more advanced M1 Abrams tank has a tank urban survival kit (TUSK) comprised of 200 mm of high-carbon steel [9]. High TUSK thickness increases the total weight of the specified tank. Composite materials are promising alternatives to traditional metallic components for lightweight vehicle protection in this regard. Since metals offer high strength and toughness accompanied by low hardness, Ceramics are a promising candidate for modifying the mechanical properties of metals due to their high hardness, high compressive strength, low density, and high fracture resistance [10].. This is because metals combine high strength and tenacity with low hardness. Blast protection can utilize a wide variety of ceramics, including alumina (Al_2O_3), Boron Carbide (B_4C), Boron Silicon Carbide (BSC), titanium diboride (TiB_2), and Silicone Carbide (SiC). Silicon carbide which identified as a typical polytypic compound consisting of nearly 200 different crystalline structures, has been accepted as the most valuable ceramic due to its prominent structural properties [11]. SiC possess lower density, superior mechanical properties especially increased hardness, higher resistance against fire and oxidation, and relatively lower cost compared to the other types of ceramics, hence it can thoroughly protect combat vehicles from intensive threat. Overall efficiency of composite V-shaped hull under blast load considerably relied on the angle of V shape plate, the composite component, and the thickness of the metal and ceramic layers. Several studies have evaluated the security of armored vehicles with modified V-shaped hull floors, but the impact of ceramic composites on the enhancement of V-shaped hull performance has not been studied. Herein, two different types of infantries fighting vehicle naming BMP-2 and BTR-80 alongside with a military truck were used as the simulation case studies. The mentioned vehicle is primarily modelled in 3D using CATIA software. Then, the Ls-dyna software was used to analyses the explosion response of these vehicles when loaded with 15 kg of trinitrotoluene (TNT). Afterward the V-shaped hull configuration of the armored vehicle was determined by the vehicle's propulsion system. An innovative composite structure consisting of Al6061-T6 and SiC were chosen as the construction material of V-shape plates. Eventually protective performance of the modified vehicle under the function of 15 kg of TNT explosion was compared to the unprotected samples. So, the effective protective function of designed V-shape configuration proved.

[Downloaded from i4c2023.iust.ac.ir on 2026-11-21]

[DOI: 10.22068/ase.2023.655]

2-Numerical Simulation:

In this investigation, the bmp-2 and btr-80 military trucks' 3D structures were designed. The length, width, and height of the designed military vehicle are 6 meters, 2.5 meters, and 3 meters, respectively and the length, width height of BMP and BTR-80 6.7 meters, 3.15 meters and 2.45 meters respectively. The aforementioned vehicle is comprised of 350,000 2D quadrilateral elements and weighs a total of 7 tones. The suspension system of this truck constituted of various components such as wheel hub, frame, axles, knuckle, shock absorber, drive shaft and etc. In addition, over 2000 constrained nodal rigid body (CNRB) have been used to connect various vehicle components. More than 500,000 3D Hexahedron elements with dimensions half that of lagrangian elements simulate the air domain. Figure 1 provides a schematic depiction of a military vehicle.it is should be noted in order to speed up the simulation, only 2D elements have been used for mentioned structured.

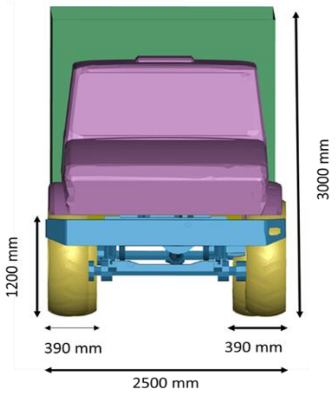


Fig. 1. schematic illustration of military truck dimension

2.1. Structures features:

Other than the assigned material models, the thickness of different parts of the structure is the second most important factor in determining the behavior of a structure under the dynamic conditions. So, thickness of various parts of the case studies abbreviated in table. In the case of the truck suspension system, the assigned thicknesses vary from 6 mm in drive axle to 2 mm in the shock absorber as well as the thickness of composite layers for all case studies is 5 mm for aluminum and ceramic layer. The thicknesses in Table.1 were based on measurements

Table 1. thickness of various parts of the case studies

Vehicle	Frontal Turret	Side turret	Hull floor	Tires	Chassis
Military Truck	213	0.295	423	9.91	6-2
BMP-2	201	0.307	424.5	10.79	-
BTR	170	0.321	291.2	11.27	-

2.2. ALE Method:

The Eulerian method, also known as the Arbitrary Lagrangian-Eulerian method or ALE, is a multi-material method that assigns a wide variety of physical parameters with great complexity. Due to its high accuracy in estimating the level of explosion devastation [12], the ALE method is regarded as the most effective simulation method for explosions that can be applied to a wide variety of structures including automobiles, buildings, etc. The (ALE) approach is more consistent with experimental data than other Explosion Simulation methodologies such as CONWEP. Contrary to conventional simulation methods, ALE simulation methods include Blast over pressure and interaction between detonated explosive charge and Armor vehicle. These benefits make the ALE method one of the most dependable simulation techniques in finite element software These advantages make ALE approach one of the most reliable simulation methods in the finite element software. The air and explosive charge were simulated using ALE methods, while the military vehicle and FV were simulated using the Laragia method [13]. In order to produce coupling interaction between eulerian and Lagrange arts, (ctype=4) used the CONSTRAINED_LAGRANGE_IN_SOLID keyword in all directions (DIREC=3). And to reduce leakage, the parameters ILEAK=2, PFAK=2, and PLEAK=2 was used. Lastly, it is important to observe that the element size of the eulerian parts must be smaller than the element size of the Laragia parts; otherwise, coupling does not occur.

[Downloaded from i4c2023.iust.ac.ir on 2026-11-21]

[DOI: 10.22068/ase.2023.655]

2.3. Equation of state (EOS):

JWL:

In nonlinear dynamic modelling employing the ALE method, the assignment of the equation of state is crucial due to the exponential increase in deformation value and strain rate. In addition, simulations of explosions must account for the propagation of shock waves in vacuum domains. Jones-Wilkins-Lee is the most well-known EOS for determining the expansion of an explosive detonate from a Chapman-Jouguet equilibrium state to a large volume. [14]. JWL EOS characterized as follow:

$$P = A\left[1 - \frac{W}{R_1}\right]e^{-R_1 V} + BA\left[1 - \frac{W}{R_{2V}}\right]e^{-R_2 V} + \frac{WE_0}{V} \quad (1)$$

Where p is the pressure, v is the ratio of the current volume to the initial volume, and *A*, B, and w are constant parameters derived from the Gunery energy. D is the same as the chapman-jouget pressure and the detonation velocity, respectively. The parameters of the JWL equation are listed in Table.2 [15]. The values of JWL equation parameters are provided in table 2.

Table 2. Jones- Wilkins Lee parameters

Ro (Kg/m^3)	D (m/s)	P_{cj} (Gp)	E_0/V (Gp)	A (Gp)	B (Gp)	R_1	R_2	W
1630	6930	21.0	7	371.213	3.2306	4.15	0.95	0.3

2.4. Linear-Polynomial:

Equation of state is required to include explosion wave reflection in numerical simulation, to compute air over pressure of volumetric domains consisting of air and water, and to estimate the expansion volume of an explosive charge [16]. Linear-Polynomial EOS, which is well-known due to its notable characteristics, is illustrated as follows:

$$P = C_0 + C_1\mu + C_2\mu^2 + C_3\mu^3 + (C_4 + C_5\mu + C_6\mu^2)E \quad (2)$$

Where C0 to C6 are the Constance coefficients, is the initial internal energy, and the gas-liquid volumetric ratio is the gas-liquid ratio. Table.3 contains the linear-polynomial equation's parameters.

Table 3. Linear-Polynomial parameters [17]

Density (Kg/m^3)	μ	C_0	C_1	C_2	C_3	C_4	C_5
1.29	1.4	0	0	0	0	0.4	0.4

3.Material Models:

3.1. J-C Damage Model for Steel Structure

Prior to the development of Composite Armored, the defense industry utilized rolled homogeneous armor (RHA). The majority of tanks and infantry combat vehicles constructed in the 20th century have RHA body structures. This article models the structure of the BMP-2 and BTR-80 using RHA specifications. Moreover, the properties of the DC04 Steel and Al-6061T6 used in the modelling of Military Truck Structure and the composite metal layer are described. In order to develop experimental stress-strain curves for metallic materials, Johnson and Cook formulated the following equation [18] [19]

$$\sigma = (A + B\varepsilon^n)\left((1 + C\mathrm{Ln}\varepsilon^*)(1 - (\frac{T - T_r}{T_m - T_r})^m\right) \quad (3)$$

In addition to strain rate and thermal effect, the J-C equation also incorporates strain rate. Three sections can be used to describe the J-C Constitutive model: quasi-static, dynamic, and thermal. Stress, hardening coefficient, hardening exponent, and plastic strain are represented by A, B, n, and correspondingly. Strain rate factor, normalized effective strain rate ratio, which is the ratio of dynamic strain rate to reference strain rate, and thermal softening coefficient are the C, m, and n parameters, respectively. T_r Refer to the temperature at which the other parameters were obtained, which is typically ambient temperature. The results of the experiments demonstrated that strain fracture in uniaxial, biaxial, shear, and uniaxial compression tests differ significantly from one another. Therefore, scientists required a computational formula to characterize this variance [20]. Applying the Triaxiality stress, which is defined as the ratio of hydrostatic stress to equivalent stress, Johnson and Cook presented their damage model. Consequently, the J-C Damage Model utilizing Stress Triaxiality is able to identify Strain Fracture

[Downloaded from i4c2023.iust.ac.ir on 2026-11-21]

[DOI: 10.22068/ase.2023.655]

in Various Dimensions. Consequently, the J-C damage material model predicts fractures with greater accuracy than piece-wise linear plasticity. The Johnson-Cook model strain fracture is defined as follows:

$$\varepsilon^{f} = \left[D_1 + D_2 e^{D_3 \sigma^*}\right][1 + D_4 \mathrm{Ln}\varepsilon^*][1 + D_5 T^*] \quad (4)$$

Damage Parameters and Mechanical Properties of an Armor Vehicle are Presented in Table 4

Table4. Johnson-cook Material Model Parameters for RHA and DC04 Steel [21, 22]

	Aluminum6061-T6	RHA	C_1
Density [*kg/m3*]	1.4	7850	7800
Poisson's Ratio	2.700	0.3	0.3
Young's Modulus, E (Gpa)	0.33	210	180
Yield stress, A (Gpa)	0.3241	0.98	0.162
hardening coefficient, *B* (Gpa)	0.1138	2	0.598
hardening exponent, *n* (Gpa	0.42	0.83	0.6
Strane rate sensitivity, *C*	0.002	0.0026	2.623
Thermal softening coefficient, m	1.34	1.4	0.009
Shear Modulus, G(Pa)	26	81.8	77
D_1	-0.77	0.5	0.02
D_2	1.45	0.8	3.9
D_3	-0.47	0.44	-4.6
D_4	0	-0.046	0.002
D_5	1.6	0	0

3.2. Johnson-Holmquist II (JH-2) model: In solid mechanics, the Johnson-Holmquist Plasticity Damage Constitutive Model is useful for modelling ceramics, glass, graphite, pebbles, concreate, and certain alloys with low plasticity strain, as well as other brittle materials. Using five distinct categories of mechanical property, the JH-2 ceramic model can evaluate the Damage Behavior of ceramics under a dynamic load. Moreover, the JH-2 model of ceramics is highly dependent on experimental data. The JH-2 model's damage mechanism consists of three distinct steps: intact, wounded, and fracture. The following equation depicts the undamaged JH-2 equation's tensile strength:

$$\sigma_1^* = \mathrm{A}(\mathrm{p}^* + \mathrm{T}^*)^{\mathrm{N}}(1 + \mathrm{C}\ln\varepsilon^*) \quad (5)$$

Where A and N are parameters of Intact normalized strength, C and E are strain rate sensitivity parameter and normalized strain rate, respectively. σ^* is also the normalized intact strength, which corresponds to the ratio of the current equivalent stress for a ceramic-type material to HEL (Hugoniot stress, which is defined as the point at which the material transitions to a plastic state). The precise value of HEL can be determined using the following equation:

$$HEL = K_1\mu_{HEL} + K_2{\mu_{HEL}}^2 + K_3{\mu_{HEL}}^3 + \frac{3}{4}G\frac{\mu_{HEL}}{1+\mu_{HEL}} \quad (6)$$

Then P^*attributed to real pressure dived to pressure component at the Hugoniot elastic limit which can be defined as follows:

$$P^* = {P}/{P_{HEL}} \quad (7)$$

And P_{HEL} assigned to the following equation:

$$P_{HEL} = K_1\mu_{HEL} + K_2\mu_{HEL}^2 + K_3\mu_{HEL}^3 \quad (8)$$

Where K_1, K_2, K_3 are Constance in elastic region and μ is the ratio of initial volume of certain component to secondary volume. $T^*$is the normalized tensile strength calculated by dividing the greatest tensile pressure strength by P_{HEL}.

$$\sigma_*^D = \sigma_1^* - D(\sigma_1^* - \sigma_F^*) \quad (9)$$

Where D is the parameter for accumulated damage Describe by the ratio of plastic strain variation to fracture plastic strain variation, the value of D located between 0 and 1, and if D factor is less than 1 the damage is assumed to be relative fracture, and when the precise amount of D parameter equals 1 the damage is referred to as total fracture. D factor determined by: Equivalent damage stress in

[Downloaded from i4c2023.iust.ac.ir on 2026-11-21]

[DOI: 10.22068/ase.2023.655]

JH-2 computational model achieved by the following equation:

$$D = \sum \frac{\Delta \varepsilon_p}{\Delta \varepsilon_P^F} \quad (10)$$

Additionally, normalized strength of fracture is given by:

$$\sigma_F^* = B(P^*)^M(1 + C ln \varepsilon^{*}) \quad (11)$$

strain rate is not essential [23]. Table 5 summarizes the Johnson-Holquist Materia Model Parameters B and m represent fracture parameters. C parameter is also considered as the strain rate effect, however, in the low plasticity region of brittle materials for Silicon Carbide

Table 5. Johnson-Holquist Materia Model Parameters for Silicon Carbide [24]

Density (Kg/m^3)	G	A	B
2510	183	0.96	0.35
C	M	EPSO	T
0.0005	1	1	0.37
SFMAX	HEL	PHEL	HEL Vol. Strain
0.8	14.567	5.9	0
D1	D2	D3	D4
0.48	0.48	0	0
K1	K2	K3	Beta
204.756	-593	2800	1

4.V-shaped Configuration:

Infantry combat vehicles are separated into two major groups: first, fighting vehicles with caterpillar treads, such as the BMP-2, and second, wheeled armored fighting vehicles, such as the LAV-25 and BTR-80. We consider two distinct design strategies based on the unique characteristics of each group. Caterpillar tread armored vehicles (CTAV) have a large steel solid chain, which has increased their resistance to mine explosions. In contrast, the suspension system of the majority of wheeled armoured vehicles is comparable to that of automobiles with run-flat tires, making them extremely vulnerable to mine and IED explosion. The mine explosion may occur precisely beneath the vehicle's wheels or hull. The conventional V-shaped hulls deflected explosion wave to the wheels, resulting in punctured tires and movement difficulties. In the present work, V-shaped plates with a novel design are used to safeguard the crew of wheeled vehicles from mine explosions. Fig.3 depicts a schematic illustration of applied multi-V-shaped plates.

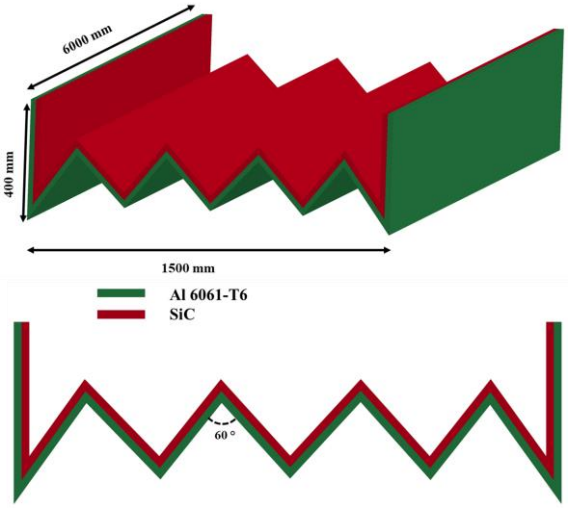


Fig. 2 Schematic illustration of Multi V-shaped for BTR and Military Truck

Traditional V-shaped design with an internal angle of 120°, as seen in bmp-2 in Figure 3. This geometry possesses remarkable advantages such as high efficiency, ease of construction, etc., making it the best option for increasing CTAV mine protection. Moreover, G.S. Langdon and coworkers demonstrated that an internal corner angle of 120 degrees significantly improves the impulse transmission and the safety potential of armored vehicles. Ceramic layer placed in outer layer of Composite

[Downloaded from i4c2023.iust.ac.ir on 2026-11-21]

[DOI: 10.22068/ase.2023.655]

Materials which are specifically constructed to resist against Armour-piercing ammunition (AP) to reduce kinematic energy of (AP)[25]. Since aluminum has a much higher plastic strain than Silicon carbide ceramic, if a composite was placed in the inner layer of the V-shape, there was a high probability of deformation inside the cabin and a threat to the lives of the occupants. Accordingly, herein Aluminum was placed in outer layer of the prepared composite, thus z-displacement of the Aluminum layer's Elements restricted [26].

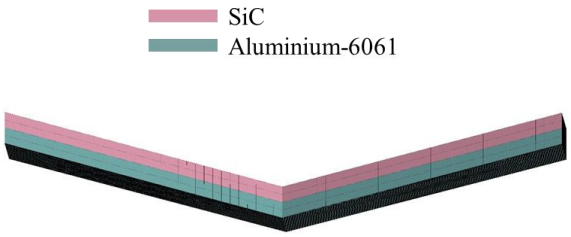


Fig. 3 Schematic illustration of Single V-shape for BMP-2

5.Results and discussion:

5.1. Military Truck:

In this section, the results of the explosion simulation of an anti-tank mine with 16 kg of TNT in two distinct modes containing with and without V-shaped plates for a military truck, BMP-2 and BTR personnel carriers have been compared with each other. Also, based on the previous reports, three basic parameters including penetrating or non-penetrating shock waves of explosives in the passenger compartment, acceleration of the center of mass of the passenger compartment and finial vertical displacement have been analyzed to evaluate the safety of the mentioned vehicles[27, 28].

Different phases of mine explosion under the military vehicle displayed in Fig. 4. explosive device demonstrated under the vehicle, near the driver in fig.4. After 1ms from the detonation of the explosive device, the blast waves developed to chassis and produced shear tension which led to the destruction of the driver shaft and causes the inability to move. In 5 ms after the explosion, the entire floor panel of the truck is affected by the blast wave and after drive shaft destruction the remainder of the chassis components such as horizontal crosses and vertical rails and axial shaft fractured. In order to cast more light on the amount of destruction, a transparency view of the 5 milliseconds following the explosion's start is provided. Clearly, the explosion waves were able to rip the steel sheets from the cabin and cargo compartment's two sections. Fig.5 depicts the acceleration that was imparted to the military occupant component's center of mass as is well known, the acceleration reaches its maximal value (277g) in 4ms, which is significantly greater than the threshold of human tolerance. (The acceleration tolerance threshold for humans is deemed to be 80g, and accelerations above this level are hazardous).

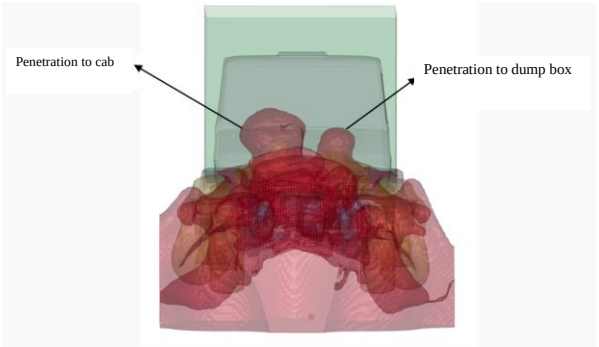


Fig. 4. Transparency view of blast wave dispersion in military truck with floor hull

The explosion simulation of a military vehicle modified with multiple V-shaped composite inclined plates containing double layers of ceramic and aluminum revealed that this design effectively deflects anti-tank mine blast waves as depicted in the fig.5, the blast waves reach the inclined plane 1.5 milliseconds after the explosion, and without having a destructive influence on the composite plane, the inclined plane begins to change its shape and departs from its initial spherical state. At 2.5 milliseconds, the blast waves completely encompass the inclined plane. Following this period, the inclined plane endures significant deformations. After that, the maximal deformation occurs in 4

[Downloaded from i4c2023.iust.ac.ir on 2026-11-21]

[DOI: 10.22068/ase.2023.655]

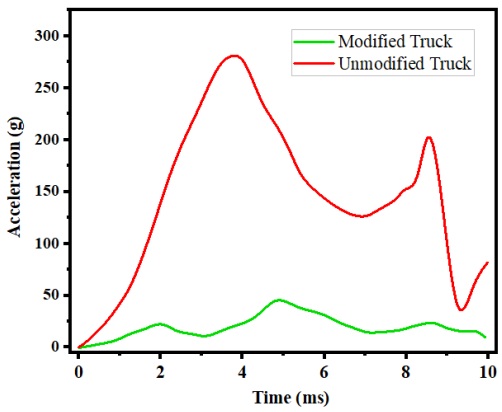


Fig.5 Comparison between occupant central mass acceleration in modified truck and un-modified truck



Fig. 6. Schematic view of Explosive device dispersion at 2.5ms.

milliseconds. As shown in fig.5, the cabin acceleration reaches a limit of 48g and then decreases exponentially.

The deformed V-shaped plate depicted in the illustration in fig.7. The detonation waves caused the inclined plate to impact the chassis and the cabin's floor panel. Thus, chassis tension has been created. Despite this, none of the chassis' components, including the drive shaft, crosses, rails, and shaft, are defective. Results demonstrated the composite inclined plate's ability to absorb and disperse the anti-tank mine detonation. Fig.6 shows Schematic view of Explosive device dispersion at 2.5ms.

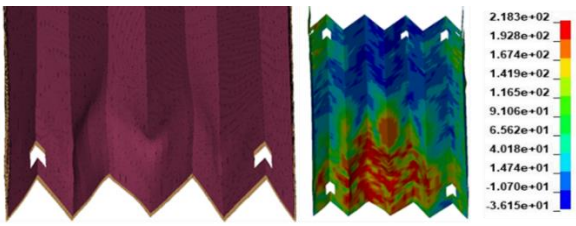


Fig.7. Schematic illustration of multi-V-shaped hull deformation

5.2.BMP-2 IFV:

Anti-tank mine containing 15 kilograms of TNT exploded beneath the BMP-2 personnel carrier, resulting in its destruction. Similar to the simulation of the explosion of the military truck, the explosion reaches the passenger structure within 1ms to 1.5ms and immediately begins destroying the elements of the lower panel of the passenger-carrier, sand, and wheels. As can be seen in the fig.10(b), a hole with a diameter of approximately 1.5m is widened between the sand on both sides of the carrier. This cavity allows extremely hot and high-velocity detonation products to enter the passenger compartment, reducing the likelihood of survival to nearly zero. Fig.10(a) depicts the fractured components of the lower panel of the passenger. In the form of shrapnel, the fragmented elements can cause double injury to the passengers. In addition, as shown in the fig.10(a), the detonation waves permeate the entire interior of the passenger carrier and, eight milliseconds after the explosion begins, exert a great deal of pressure on the turret in the direction of the explosion, causing a change in its shape. The plastic expands the turret, but due to the immense thickness of the turret, it is unable to separate the turret from the body. As a result, the explosion waves return from the turret into the passenger compartment, bending and shattering all the metal sheets on the turret. Discrete In 10 milliseconds after the explosion begins, due to the depletion of TNT, the explosion waves will disperse and no further devastation will occur. Due to the armored character of the BMP-2, it will never be able to withstand anti-tank mines, and extensive destruction of

[Downloaded from i4c2023.iust.ac.ir on 2026-11-21]

[DOI: 10.22068/ase.2023.655]

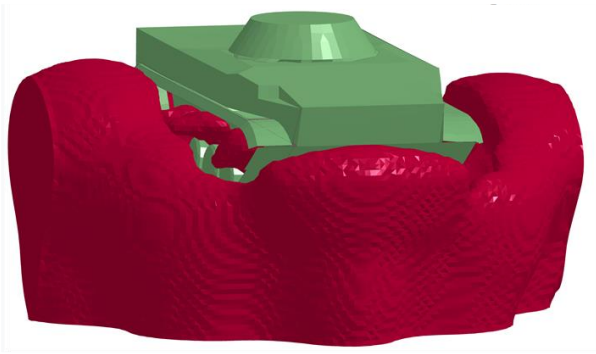


Fig. 8. Schematic Illustration of blast wave desperation through the BMP-2

the personnel carrier is both inevitable and unavoidable.

Examining the data of the modified BMP-2 model with an inclined plane reveals that there was no penetration into the passenger compartment, only the sands and a portion of the side structure of the people carrier were destroyed, and the acceleration of the people carrier's center of mass reaches its maximum value. Maximum acceleration of the mass center is 38,5g, demonstrating the high safety of the optimization, and the image below depicts the average stress applied to this inclined composite plate. Due to the armored nature of the BMP-2, the V-shaped composite inclined surface design is significantly more effective at dispersing explosion waves. Fig.8 Schematic Illustration of blast wave desperation through the BMP-2.

Fig.9 Showes the Central mass acceleration of Modified bmp-2 Compered to Un-Modified BMP-2

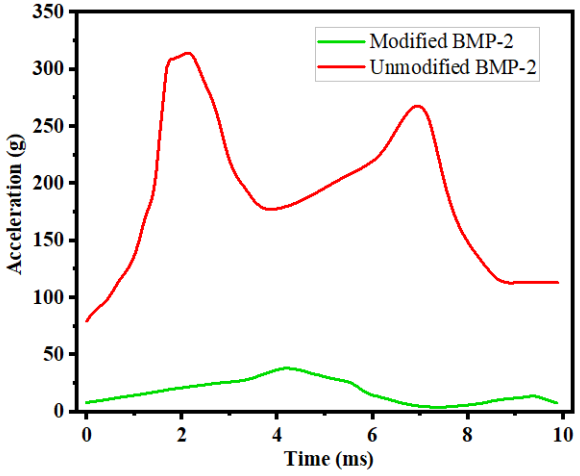


Fig.9. Central mass acceleration of Modified bmp-2 Compered to Un-Modified BMP-2

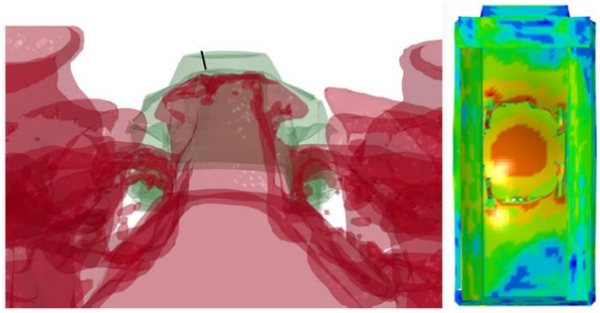


Fig.10. (a)-Transparency Schematic illustration of blast wave depression Through un-modified BMP-2, (b)-view of floor hull ofbmp-2 After explosion

5.3.BTR-80 IFV:

Since the BTR personnel carrier, unlike the BMP-2 personnel carrier, lacks a suitable armor structure, the anti-tank mine utterly destroys the structure of this personnel carrier upon impact. Immediate damage is caused to the tires and suspension system by blast waves, which then penetrate the bottom panel and infiltrate the passenger cabin. As shown in the fig.11, 4 milliseconds after the explosion, the entire carrier is covered with explosion debris, and because the overall thickness of the BTR structure is small, the blast waves are not dissipated like they are in the BMP-2 carrier. As a result, the blast waves enter the turret, the pressure inside the turret increases exponentially, and the turret separates from the rear of the carrier.



Fig.11.Transparency Schematic illustration of wave blast depression trough BTR-80 IFV.

In addition, numerous components of the upper body may also fail. The figure below depicts the average vertical acceleration of the turret elements at the site of attachment to the body, as it is evident that the acceleration value reaches a very high value of 700g. Therefore, obbious that survival is impossible under these conditions. By comparing the three research cases in this article, it is evident

[Downloaded from i4c2023.iust.ac.ir on 2026-11-21]

[DOI: 10.22068/ase.2023.655]

that the anti-tank mine detonation was able to penetrate the structures of all three, but that the condition of the TR carrier was significantly worse.

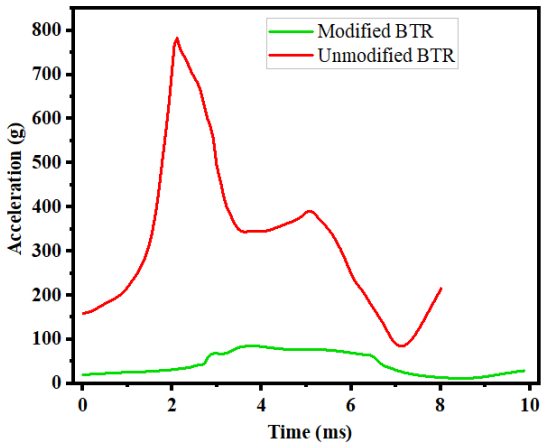


Fig.12. Central mass acceleration of Modified BTR-80 Compered to Un-Modified BTR-80.

The multiple V inclined plate used in the military truck (based on Benz 911 vehicle) has been redesigned for use in the BTR passenger carrier in order for it to be re-used in the new structure. Considering the nature and function of the BTR to traverse a variety of impediments, the design of the multiple V-shaped plate covers only half of the tires so as not to hinder the BTR's mobility. When an explosion strikes a flat inclined plate, a great deal of stress is introduced, after which the aluminum layer enters the plastic region and changes its shape permanently. This causes a local fracture in the ceramic layer of the composite inclined plate, Fig.12 illustrated Central mass acceleration of Modified BTR-80 Compered to Un-Modified BTR-80. In the table 5, the amount of the maximum global z-displacement and velocity occurs for three case studies in two modified and non-modified states is shown. In maximum velocity and displacement parameters, both in modified and un-modified mode, the worst performance was for BTR-80 IFV and the best performance was for BMP-2, The military truck is also placed in a suitable position with results close to the BMP-2 .The main reason is that due to the solid suspension and chassis of the truck, the blast waves are significantly weakened before reaching the passenger cabin. By placithe modified truck we have seen a 39.2% improvement in Z-displacement and a 55% improvement in vertical velocity. This amount is equal to 39.07 and 61.09 for BMP-2 and %37.5 and %39.52 for BTR, respectively.

Table 6. comparison of variation displacement and velocity in modified and un-modified models

Model	Truck	BMP-2	BTR-80
Unmodified Max Global Z - Displacement	62.5	65	120
Modified Max Global Z-Displacement	38	39.6	75
Modified Max Z-Velocity	45	96	183
Unmodified Maz Z-Velocity	110	155	256

6.Conclusion:

The use of ceramic composite plates has resulted in a significant weight reduction and a very high reliability factor for armored vehicles. The result of examining 2 of the most important safety parameters in the discussion of explosion for all three armored vehicles demonstrates that the modified samples with a composite inclined plate have completely repelled the explosion of an anti-tank mine, but in the meantime, the BMP-2 IFV due to More armor and the occupants of continues tracks vehicle and had a much better performance, followed by the military truck, which is classified as a transport vehicle. And at the end of the BTR carrier in the unmodified sample, the turret is torn off, whereas in the modified sample, the identical gene recorded the greatest acceleration of the center of mass.

[Downloaded from i4c2023.iust.ac.ir on 2026-11-21]

[DOI: 10.22068/ase.2023.655]

7.Reference

[1] V. Babu, R. Thyagarajan, and J. Ramalingam, "Faster method of simulating military vehicles exposed to fragmenting underbody IED threats," SAE Technical Paper, 0148-7191, 2017.

[2] J. G. Rasico, C. A. Newman, and M. R. Jensen, "Modelling fragmentation of a 155 mm artillery shell IED in a buried mine blast event," International journal of vehicle performance, vol. 4, no. 4, pp. 323-346, 2018.

[3] W. Jiang, N. Vlahopoulos, M. P. Castanier, R. Thyagarajan, and S. Mohammad, "Tuning material and component properties to reduce weight and increase blastworthiness of a notional V-hull structure," Case Studies in Mechanical Systems and Signal Processing, vol. 2, pp. 19-28, 2015.

[4] G. Langdon, A. Curry, and A. Siddiqui, "Improving the impulse transfer and response characteristics of explosion loaded compound angle V-plates," Thin-Walled Structures, vol. 148, p. 106609, 2020.

[5] D. Makwana, D. Thakur, and K. Senthilkumar, "Numerical analysis and effects on rigidity of combat vehicle structure due to blast load," Procedia Structural Integrity, vol. 14, pp. 44-52, 2019.

[6] J. Trajkovski, J. Perenda, and R. Kunc, "Blast response of Light Armoured Vehicles (LAVs) with flat and V-hull floor," Thin-Walled Structures, vol. 131, pp. 238-244, 2018.

[7] A. Mohamed, M. El-Gindy, and J. Ren, "Advanced control techniques for unmanned ground vehicle: literature survey," International journal of vehicle performance, vol. 4, no. 1, pp. 46-73, 2018.

[8] J. Bidadi, H. Hampaiyan Miandowab, and H. Saeidi Googarchin, "Experimental and Numerical Investigation of the Performance of Automotive Adhesively Bonded Crash Box Beams Under Transverse Loading," Automotive Science and Engineering, vol. 13, no. 2, pp. 4085-4091, 2023.

[9] M. Cong, Y.-b. Zhou, M. Zhang, X.-w. Sun, C. Chen, and C. Ji, "Design and optimization of multi-V hulls of light armoured vehicles under blast loads," Thin-Walled Structures, vol. 168, p. 108311, 2021.

[10] A. Erdik, "Experimental and numerical study on dynamic response of V-shaped hull subjected to mine blast," Mechanics based design of structures and machines, vol. 50, no. 2, pp. 707-725, 2022.

[11] A. Erdik, N. Kilic, M. Guden, and A. Tasdemirci, "Numerical approach to design process of armored vehicles," in Engineering Systems Design and Analysis, 2010, vol. 49187, pp. 231-237.

[12] J. Trajkovski, "Comparison of MM-ALE and SPH methods for modelling blast wave reflections of flat and shaped surfaces," in Proceedings of the 11th European LS-Dyna Conference, Salzburg, Austria, 2017, pp. 9-11.

[13] J. M. Puryear, D. J. Stevens, K. A. Marchand, E. B. Williamson, and C. K. Crane, "ALE modeling of explosive detonation on or near reinforced-concrete columns," in Proceedings of the 12th International LS-DYNA Users Conference, Detroit, MI, USA, 2012, pp. 3-5.

[14] Z. S. Tabatabaei and J. S. Volz, "A comparison between three different blast methods in LS-DYNA: LBE, MM-ALE, Coupling of LBE and MM-ALE," in 12th International LS-DYNA Users Conference, 2012, no. 3, pp. 1-10.

[15] G. Baudin and R. Serradeill, "Review of Jones-Wilkins-Lee equation of state," in EPJ Web of Conferences, 2010, vol. 10: EDP Sciences, p. 00021.

[16] D.-M. Bae and A. F. Zakki, "Comparisons of multi material ALE and single material ALE in LS-DYNA for estimation of acceleration response of free-fall lifeboat," Journal of the Society of Naval Architects of Korea, vol. 48, no. 6, pp. 552-559, 2011.

[17] M. E. Korkmaz, "Verification of Johnson-Cook parameters of ferritic

[Downloaded from i4c2023.iust.ac.ir on 2026-11-21]

[DOI: 10.22068/ase.2023.655]

stainless steel by drilling process: experimental and finite element simulations," Journal of Materials Research and Technology, vol. 9, no. 3, pp. 6322-6330, 2020.

[18] F. Dolce, M. Meo, A. Wright, M. French, and M. Bernabei, "Hybrid S2/carbon epoxy composite armours under blast loads," Applied Composite Materials, vol. 19, pp. 349-362, 2012.

[19] A. Banerjee, S. Dhar, S. Acharyya, D. Datta, and N. Nayak, "Determination of Johnson cook material and failure model constants and numerical modelling of Charpy impact test of armour steel," Materials Science and Engineering: A, vol. 640, pp. 200-209, 2015.

[20] M. Jutras, "Improvement of the characterisation method of the Johnson-Cook Model," Citeseer, 2008.

[21] M. Gerstgrasser et al., "Analysis of two parameter identification methods for original and modified Johnson-Cook fracture strains, including numerical comparison and validation of a new blue-brittle dependent fracture model for free-cutting steel 50SiB8," Theoretical and Applied Fracture Mechanics, vol. 112, p. 102905, 2021.

[22] S. Akram, S. H. I. Jaffery, M. Khan, M. Fahad, A. Mubashar, and L. Ali, "Numerical and experimental investigation of Johnson–Cook material models for aluminum (Al 6061-T6) alloy using orthogonal machining approach," Advances in Mechanical Engineering, vol. 10, no. 9, p. 1687814018797794, 2018.

[23] P. R. S. Reddy, S. G. Savio, and V. Madhu, "Ceramic composite armour for ballistic protection," Handbook of *Advanced Ceramics and Composites: Defense, Security, Aerospace and Energy Applications,* pp. 357-402, 2020.

[24] M. Xu *et al.*, "Recent advances and challenges in silicon carbide (SiC) ceramic nanoarchitectures and their applications," *Materials Today Communications,* vol. 28, p. 102533, 2021.

[25] F. Yang *et al.*, "Mechanical and oxidation properties of C/SiC corrugated lattice core composite sandwich panels," *Composite Structures,* vol. 158, pp. 137-143, 2016.

[26] R. Klement, S. Rolc, R. Mikulikova, and J. Krestan, "Transparent armour materials," *Journal of the European Ceramic Society,* vol. 28, no. 5, pp. 1091-1095, 2008.

[27] A. Ramasamy, A.-M. Hill, A. Hepper, A. M. Bull, and J. C. Clasper, "Blast mines: physics, injury mechanisms and vehicle protection," *BMJ Military Health,* vol. 155, no. 4, pp. 258-264, 2009.

[28] S. Anas, M. Alam, and M. Umair, "Air-blast and ground shockwave parameters, shallow underground blasting, on the ground and buried shallow underground blast-resistant shelters: a review," *International Journal of Protective Structures,* vol. 13, no. 1, pp. 99-139, 2022.

[Downloaded from i4c2023.iust.ac.ir on 2026-11-21]

[DOI: 10.22068/ase.2023.655]